10.1109/ULTSYM.2009.0530

PZT transduced high-overtone width-extensional resonators above 1 GHz

Hengky Chandrahalim
and Sunil A. Bhave
School of Electrical and
Computer Engineering
Cornell University
Ithaca, New York 14853, USA

Ronald G. Polcawich,
Jeffrey S. Pulskamp,
and Roger Kaul
US Army Research Laboratory
Adelphi, MD 20783, USA

***Abstract*—This paper provides the theoretical modeling, simulation, and quantitative comparison that explore the design space of PZT-only (Lead Zirconate Titanate) and PZT-on 3, 5 and 10 μm single-crystal silicon high-overtone width-extensional mode (WEM) resonators with identical lateral dimensions for incorporation into radio frequency microelectromechanical systems (RF MEMS) filters and oscillators. A novel fabrication technique was developed to fabricate the resonators with and without silicon layer using the same mask-set on the same wafer. The air-bridge metal routings were implemented to carry electrical signals while avoiding large capacitances from the bond-pads. We theoretically verified and experimentally measured the correlation of motional impedance (R_X), quality factor (Q), and resonance frequency (f) with the resonators' silicon layer thickness (t_{Si}) up to above 1 GHz frequency of operation. For identical lateral dimensions and PZT-layer thickness (t_{PZT}), the resonators with thicker silicon layer have higher f. The resonators with thicker silicon also have higher Q and lower R_X up to 900 MHz frequency.**

I. Introduction

The development of modern integrated wireless communication systems has pushed the investigation of efficient electromechanical transducer materials for micro-electromechanical resonators and filters. Aluminum nitride (AlN) is a favorable material for UHF and SHF applications because it possesses a high acoustic velocity, high quality factor and post-CMOS integration capability [1], [2]. However, ferroelectric materials such as PZT are better suited for devices that operate at HF up to UHF range as they avoid thick film requirements and reduce the area required for the resonators and filters. Furthermore, PZT exhibits larger electromechanical coupling coefficient than AlN, enabling the design of larger $\%$ bandwidth filters [3]. PZT is also an attractive electromechanical transducer because it possesses a DC bias dependent elastic modulus. This property has been utilized to design PZT transduced length-extensional mode (LEM) resonators with up to 5% frequency tuning [4]. However, PZT-only resonators are well known to have low-Q. In order to overcome the low-Q of PZT-only resonators, we developed a new fabrication technology to integrate PZT transduction with single-crystal silicon (SCS) resonators. This fabrication technology allows to fabricate PZT-only and PZT-on-silicon resonators using the same mask-set on the same wafer.

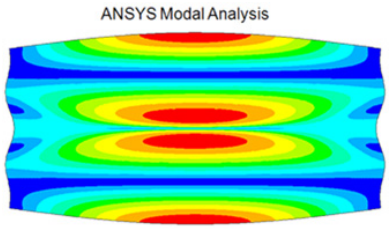

Fig. 1. ANSYS mode shape of a high-overtone width-extensional mode resonator.

PZT transduced LEM resonators have been successfully demonstrated. By varying the silicon thickness, t_{Si} (thereby the % mass of crystalline silicon in the resonator) and DC bias voltage we can define the desired Q and frequency tuning range of the resonators [4]. However, various applications in wireless communication systems demand for higher frequency of operation. In order to reach f above 100 MHz using length-extensional mode of vibration, the length of PZT-on-silicon resonator has to be scaled down to less than 40 μm. The length of PZT-only resonators has to be shrunk even more due to a lower acoustic velocity. Aggressive scaling in lateral dimensions of the resonator reduces the transduction area resulting in poor motional impedances. In order to enable PZT transduced resonators with a high frequency of operation while maintaining a low motional impedance, design and fabrication of PZT transduced high-overtone width-extensional mode (WEM) resonators will be presented.

II. High-overtone WEM Resonator

A. Design of a High-overtone WEM Resonator

A high-overtone width-extensional mode of vibration can be excited to achieve a high resonance frequency while utilizing a large transduction area [5]. By selectively patterning the interdigitated electrodes on top of the resonators the higher-overtone of width extensional mode is excited as demonstrated in ANSYS modal analysis in Figure 1.

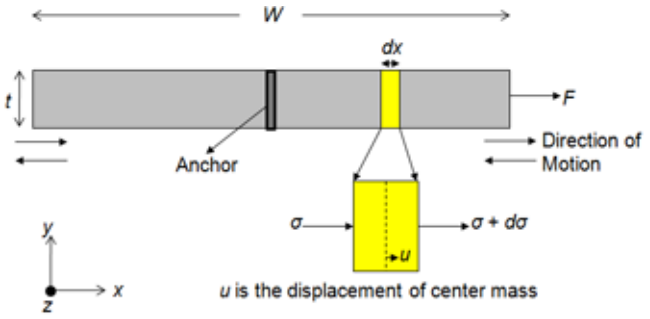

Fig. 2. The cross-section view of a width-extensional mode resonator.

B. Effective Mass, Damping Ratio, and Effective Spring Constant

The cross-section view of a WEM resonator with width, W and thickness, t is shown in Figure 2. The resonator vibrates in the direction normal to area, A (not shown in the picture). From Newton's law of motion, the sum of forces that act on the resonator can be expressed as

$$(\sigma(x,t) - d\sigma(x,t))\, A - \sigma(x,t)A = \rho A dx \frac{\partial^2 u(x,t)}{\partial t^2} \quad (1)$$

Equation 1 can be written as

$$A\frac{\partial \sigma(x,t)}{\partial x} = \rho A \frac{\partial^2 u(x,t)}{\partial t^2} \quad (2)$$

$$A\frac{\partial E\frac{\partial u(x,t)}{\partial x}}{\partial x} = \rho A \frac{\partial^2 u(x,t)}{\partial t^2} \rightarrow EA\frac{\partial^2 u(x,t)}{\partial x^2} = \rho A \frac{\partial^2 u(x,t)}{\partial t^2} \quad (3)$$

where E is the Young's modulus of the structure. The wave equation for a one-dimensional vibrating length-extensional mode resonator including the damping factor and external forces is

$$\rho A\frac{\partial^2 u}{\partial t^2}(x,t) - bA\frac{\partial}{\partial t}\frac{\partial^2 u}{\partial x^2}(x,t) - EA\frac{\partial^2 u}{\partial x^2}(x,t) = \frac{\partial f}{\partial t}(x,t) \quad (4)$$

By the method of separation of variables, we assume equation 4 has solutions of the form

$$u(x,t) = g(t)\sin\left(\frac{n\pi}{W}x\right) \quad (5)$$

Substituting 5 into 4 gives

$$\begin{aligned} &\rho A \sin\left(\tfrac{n\pi}{W}x\right)\tfrac{\partial^2 g(t)}{\partial t^2} + bA\left(\tfrac{n\pi}{W}\right)^2 \sin\left(\tfrac{n\pi}{W}x\right)\tfrac{\partial g(t)}{\partial t} \\ &+EA\left(\tfrac{n\pi}{W}\right)^2 \sin\left(\tfrac{n\pi}{W}x\right) g(t) = \tfrac{\partial f}{\partial t}(x,t) \end{aligned} \quad (6)$$

Multiply 6 by $\sin\left(\frac{n\pi}{W}x\right)$ and integrate over the length yields

$$\begin{aligned} &\int_{-W/2}^{W/2} \rho A\left(\sin\left(\tfrac{n\pi}{W}x\right)\right)^2 \tfrac{\partial^2 g(t)}{\partial t^2} + bA\left(\tfrac{n\pi}{W}\right)^2\left(\sin\left(\tfrac{n\pi}{W}x\right)\right)^2 \tfrac{\partial g(t)}{\partial t} \\ &+EA\left(\tfrac{n\pi}{W}\right)^2\left(\sin\left(\tfrac{n\pi}{W}x\right)\right)^2 g(t)dx = F(t) \end{aligned} \quad (7)$$

Equation 7 can be simplified as

$$\frac{\rho AW}{2}\frac{\partial^2 g(t)}{\partial t^2} + \frac{bAW}{2}\left(\frac{n\pi}{W}\right)^2\frac{\partial g(t)}{\partial t} + \frac{EAW}{2}\left(\frac{n\pi}{W}\right)^2 g(t) = F(t) \quad (8)$$

From equation 8, we can recognize the effective mass, damping ratio and effective spring constant of a width-extensional mode resonator with width W are given by

$$M_{Eff} = \frac{\rho AW}{2} \quad (9)$$

$$\zeta = \frac{bAW}{2}\left(\frac{n\pi}{W}\right)^2 = \frac{n^2 bA\pi^2}{2W} \quad (10)$$

$$K_{Eff} = \frac{EAW}{2}\left(\frac{n\pi}{W}\right)^2 = \frac{n^2 EA\pi^2}{2W} \quad (11)$$

C. Electromechanical Coupling Coefficient

The lateral stress, σ in PZT is governed by the constitutive equation

$$\sigma = E\epsilon - e_{31}\frac{v_{AC}}{t} \quad (12)$$

where ϵ, e_{31}, E and t are the strain, transverse piezoelectric stress constant, Young's Modulus and thickness of PZT respectively. If the PZT is free to deform, the total stress is zero, and equation 12 becomes

$$0 = E\epsilon - e_{31}\frac{v_{AC}}{t} \quad (13)$$

and the strain ϵ is

$$\epsilon = \frac{e_{31}}{E}\frac{v_{AC}}{t} \quad (14)$$

The piezoelectric force, F_{PZT} due to PZT transduction is

$$F_{PZT} = \epsilon EA = e_{31}A\frac{v_{AC}}{t} \quad (15)$$

where A is the cross sectional area orthogonal to direction of motion. By substituting e_{31} with d_{31} x E, equation 15 can be written as

$$F_{PZT} = 2\ d_{31}\ E\ L_{PZT}\ v_{AC} \quad (16)$$

The efficiency of electromechanical transduction by PZT is indicated by the electromechanical coupling constant η.

$$\eta = \frac{F_{PZT}}{v_{AC}} = 2\ d_{31}\ E\ L_{PZT} \quad (17)$$

D. Small-signal electrical equivalent circuit

The effective mass, damping ratio and effective spring constant can be related in to electrical circuit parameters. By substituting $\frac{\partial g(t)}{\partial t}$ in 8 by $\frac{i(t)}{\eta}$, we obtain

$$\frac{M_{Eff}}{\eta}\frac{\partial i(t)}{\partial t} + \frac{\zeta}{\eta}i(t) + \frac{K_{Eff}}{\eta}\int i(t)dt = F(t) \quad (18)$$

or

$$\frac{M_{Eff}}{\eta^2}\frac{\partial i(t)}{\partial t} + \frac{\zeta}{\eta^2}i(t) + \frac{K_{Eff}}{\eta^2}\int i(t)dt = v(t) \quad (19)$$

From 19 we can define the motional resistance, capacitance and inductance of the 2-port PZT-only transduced high-overtone WEM resonator. The small signal electrical equivalent impedances a PZT-only transduced high-overtone WEM resonator are

$$R_{X\_PZT-only} = \frac{\pi}{n4Q}\frac{{\rho_{PZT}}^{\frac{1}{2}}}{{E_{PZT}}^{\frac{3}{2}}}\frac{t_{PZT}}{L_{PZT}}\frac{1}{{d_{31}}^2} \quad (20)$$

$$C_{X\_PZT-only} = \frac{4}{n\pi^2}\frac{L_{PZT}W}{t_{PZT}}E_{PZT}{d_{31}}^2 \quad (21)$$

$$L_{X\_PZT-only} = \frac{n\rho_{PZT}}{{E_{PZT}}^2}\frac{t_{PZT}W}{L_{PZT}}\frac{1}{4{d_{31}}^2} \quad (22)$$

Using the identical line of derivation, the motional resistance, capacitance and inductance of the 2-port PZT-on-silicon transduced resonator are given by

$$R_{X\_PZT-on-Si} = \frac{\pi}{n4Q}\frac{\rho_{Eff}{}^{\frac{1}{2}}E_{Eff}{}^{\frac{1}{2}}}{{E_{PZT}}^2}\frac{(t_{Si}+t_{PZT})}{L_{PZT}}\frac{1}{{d_{31}}^2} \quad (23)$$

$$C_{X\_PZT-on-Si} = \frac{4}{n\pi^2}\frac{L_{PZT}W}{(t_{Si}+t_{PZT})}\frac{{E_{PZT}}^2}{E_{Eff}}{d_{31}}^2 \quad (24)$$

$$L_{X\_PZT-on-Si} = \frac{n\rho_{Eff}}{{E_{PZT}}^2}\frac{(t_{Si}+t_{PZT})W}{L_{PZT}}\frac{1}{4{d_{31}}^2} \quad (25)$$

where ρ_{Eff} and E_{Eff} are the effective (PZT + Silicon) density and Young's modulus, L_{PZT} is the length of PZT transducer under the input electrode, d_{31} is the transverse piezoelectric coefficient, and ρ_{PZT} and E_{PZT} are the density and Young's modulus of the PZT thin-film.

III. Fabrication Process

The device fabrication is largely based on the fabrication sequence outlined in [4] with additional improvements in the process to eliminate the pad capacitances. PZT is well known to have a large permittivity that can lead into large pad capacitances. Therefore, in this refined fabrication process, the air-bridge metal routings were implemented to carry electrical signals while avoiding large capacitances from the bond-pads. In addition, a novel fabrication technique was developed to fabricate the resonators with and without silicon layer using the same mask-set on the same wafer. A systematic study is essential to investigate the effect of silicon on Q, f, and R_X of PZT transduced resonators at radio frequency. In this research effort, we fabricated PZT-only and PZT-on 3, 5 and 10 μm SCS high-overtone width-extensional mode resonators with identical lateral dimensions.

A thin elastic layer of SiO_2 and a PZT actuator comprised of Ti/Pt/PZT/Pt were deposited on SOI wafers with 3 μm, 5 μm and 10 μm thick device layer and 250 nm of buried oxide. The PZT films were deposited using a chemical solution deposition method with a crystallization temperature of 700 °C to achieve full densification and high crystallinity. The input and output terminals of the resonators are lithographically defined by patterning the top Pt electrode on top of the PZT actuator. The current configuration of the resonator uses a common bottom Pt electrode underneath of the PZT for both the input and output ports. The process cross-section of released PZT-on-silicon and PZT-only resonators is shown in Figure 3. To ensure survival of the SCS (single crystal silicon) component of the resonators, an organic photo-definable layer was developed to provide protection of the resonator while allowing undercutting of the handle wafer silicon using a XeF_2 etch. At the end of device fabrication, the PZT film already possesses some degree poling as a result of the plasma processing. In order to improve the degree of poling, the resonators were subjected to electric fields of 200 kV/cm for 10 minutes prior to testing. SEM images of released PZT-on-silicon and PZT-only filters are shown in Figure 4.

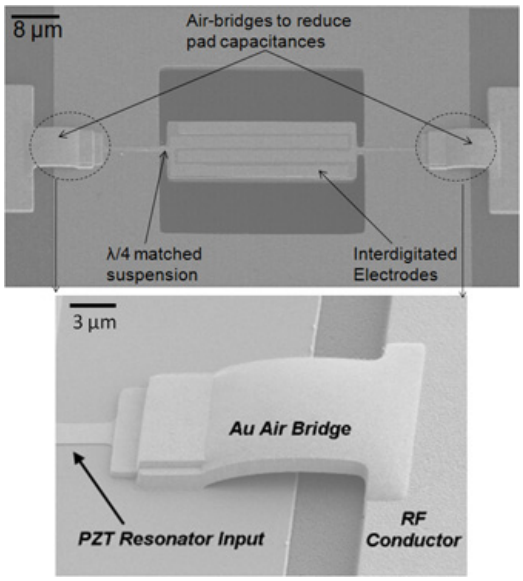

Fig. 4. SEM image of the fabricated high-overtone width-extensional mode resonator. The zoom-in picture shows the air-bridge routing that isolates the resonator from the bonding-pads.

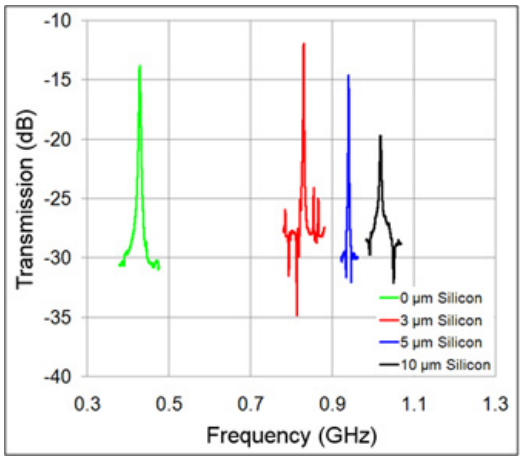

Fig. 5. Measured transmission response of PZT-only and PZT on 3 μm, 5 μm and 10 μm silicon resonators with the exact same lateral dimensions in air at room temperature and pressure. All measurements were performed using termination impedances (R_L) of 50 Ω.

IV. Characterization of High-overtone WEM Resonators

The resonators were characterized in an RF probe station in a 2-port configuration using GSG probes. Parasitics up to the probe tips were first calibrated with SOLT measurements on a standard calibration substrate. All measurements were performed in air, at room temperature and pressure. The trade-offs in Q, f and R_X of resonators with different silicon thicknesses were recorded. Resonators with thicker silicon

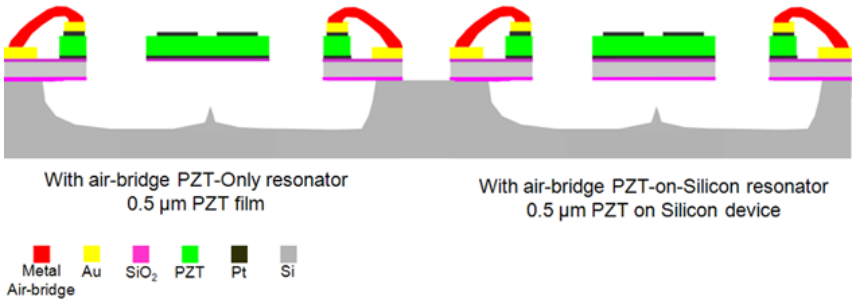

Fig. 3. Air-bridge process cross-section of PZT-only and PZT-on-silicon high-overtone width-extensional mode resonators fabricated on the same wafer.

TABLE I
THE MEASURED CHARACTERISTICS OF HIGH-OVERTONE WEM RESONATORS WITH DIFFERENT SILICON THICKNESSES

t_{Si} (μm)	0	3	5	10
Q	150	314	501	458
f (MHz)	428	834	942	1,018
R_X (Ω)	390	296	435	700
R_L (Ω)	50	50	50	50
f x Q	6.4x10^{10}	2.6x10^{11}	4.6x10^{11}	4.7x10^{11}

layer exhibit higher Q, higher f and lower R_X for frequency up to about 900 MHz as shown in Figure 5. The loss-tangent of PZT starts to dominate the insertion loss and degrade the quality factor for frequency of operation above 1 GHz. The measured characteristics of the high-overtone WEM resonators with different silicon thicknesses are summarized in Table I.

The measured resonance frequency of the resonators with different silicon thicknesses are in agreement with the theoretically analyzed and simulated data. Figure 6 plotted the calculated, simulated and measured resonance frequency of PZT transduced high-overtone WEM resonators with different silicon thicknesses (t_{Si}). By integrating PZT transduction with single-crystal silicon the figure of merit, f x Q is improved by one order of magnitude.

V. CONCLUSION

In conclusion, we have fabricated PZT transduced high-overtone WEM resonators with and without silicon device layer using the same mask on the same wafer. A novel fabrication technique has been developed to allow cancelation of large pad capacitances. The BVD models for PZT-only and PZT-on-silicon high-overtone WEM resonators have been derived and used to design resonators with frequency above 1 GHz. The performances of PZT transduced high-overtone WEM resonators with various silicon thicknesses were investigated. Integrating PZT transduction with silicon improves the f x Q by one order of magnitude. Frequency of operation is dominated by the silicon layer for silicon thickness larger than 3 μm. By varying the silicon thickness we can define the desired Q and center frequency of the resonators from high

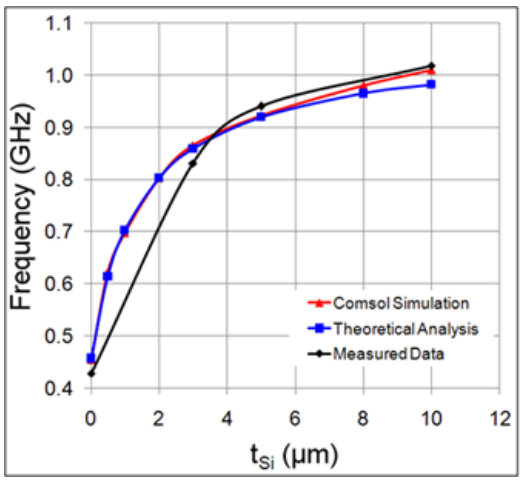

Fig. 6. A plot of silicon thickness (t_{Si}) vs the calculated, simulated and measured resonance frequency (f_C).

frequency up to ultra high frequency range. This technology will enable PZT transduced resonators, filters, and oscillators that covers up to low-band GSM frequencies.

ACKNOWLEDGMENT

The authors would like to thank Brian Power, Joel Martin and Richard Piekarz of the Army Research Laboratory for their assistance in fabricating the resonators.

REFERENCES

[1] R. C. Ruby, A. Barfknecht, C. Han, Y. Desai, F. Geefay, G. Gan, M. Gat, and T. Verhoeven, "High-Q FBAR filters in a wafer-level chip-scale package," *Digest of Technical Papers - IEEE International Solid-State Circuits Conference* , pp. 184 – 185, (San Francisco, CA, United states), 2002.

[2] G. Piazza, "Integrated aluminum nitride piezoelectric microelectromechanical system for radio front ends," *Journal of Vacuum Science and Technology A: Vacuum, Surfaces and Films* **27**(4), pp. 776 – 784, 2009.

[3] J. D. Larson III, S. R. Gilbert, and B. Xu, "PZT Material properties at UHF and microwave frequencies derived from FBAR measurements," *Proceedings - IEEE Ultrasonics Symposium* **1**, pp. 173 – 177, (Montreal, Que., Canada), 2004.

[4] H. Chandrahalim, S. A. Bhave, R. Polcawich, J. Pulskamp, D. Judy, R. Kaul, and M. Dubey, "Performance comparison of $Pb(Zr_{0.52}Ti_{0.48})O_3$-only and $Pb(Zr_{0.52}Ti_{0.48})O_3$-on-silicon resonators," *Applied Physics Letters* **93**(23), p. 233504, 2008.

[5] G. K. Ho, R. Abdolvand, and F. Ayazi, "High-order composite bulk acoustic resonators," *Proceedings of the IEEE International Conference on Micro Electro Mechanical Systems (MEMS)* , pp. 791 – 794, (Kobe, Japan), 2007.